Review of Scientific Instruments

Reflector automatic acquisition and pointing based on auto-collimation theodolite

Cite as: Rev. Sci. Instrum. **89**, 015101 (2018); https://doi.org/10.1063/1.4986313
Submitted: 04 June 2017 . Accepted: 16 October 2017 . Published Online: 02 January 2018

Jun Luo, Zhiqian Wang, Zhuoman Wen, Mingzhu Li, Shaojin Liu, and Chengwu Shen

Reflector automatic acquisition and pointing based on auto-collimation theodolite

Jun Luo,[1] Zhiqian Wang,[2,a)] Zhuoman Wen,[3] Mingzhu Li,[4] Shaojin Liu,[2] and Chengwu Shen[2,5]
[1]*Institute of Optics and Electronics, Chinese Academy of Sciences, Chengdu 610209, China*
[2]*Changchun Institute of Optics, Fine Mechanics and Physics, Chinese Academy of Sciences, Changchun 130033, China*
[3]*Southwest China Research Institute of Electronic Equipment, China Electronics Technology Group Corporation, Chengdu 610036, China*
[4]*Shanghai Huizhong Automotive Manufacturing Co., Ltd., Shanghai 200122, China*
[5]*University of Chinese Academy of Sciences, Beijing 100049, China*

(Received 4 June 2017; accepted 16 October 2017; published online 2 January 2018)

An auto-collimation theodolite (ACT) for reflector automatic acquisition and pointing is designed based on the principle of autocollimators and theodolites. First, the principle of auto-collimation and theodolites is reviewed, and then the coaxial ACT structure is developed. Subsequently, the acquisition and pointing strategies for reflector measurements are presented, which first quickly acquires the target over a wide range and then points the laser spot to the charge coupled device zero position. Finally, experiments are conducted to verify the acquisition and pointing performance, including the calibration of the ACT, the comparison of the acquisition mode and pointing mode, and the accuracy measurement in horizontal and vertical directions. In both directions, a measurement accuracy of ±3″ is achieved. The presented ACT is suitable for automatic pointing and monitoring the reflector over a small scanning area and can be used in a wide range of applications such as bridge structure monitoring and cooperative target aiming. *Published by AIP Publishing.* https://doi.org/10.1063/1.4986313

I. INTRODUCTION

A theodolite is a precision instrument for angle determination in horizontal and vertical planes. Using its optical beam and two rotary encoders, the angles between the optical axis and the zero position of the encoders are measured. Nowadays, the widely used total station upgrades the theodolite by increasing the distance measurement function. A total station can be taken as a theodolite when its angle measurement function is activated. With the assistance of the optical beam, theodolites offer the merit of contactless measurements with high precision. Therefore, optical measurements based on theodolites have gained a lot of attention and have been employed in many fields.

Some studies have provided the methods to calibrate theodolites. A calibration method for the vertical angle measuring system of a total station using horizontal angle calibration means was presented.[1] Subsequently, a trigonometric vertical angle calibration approach of the total station was put forward, and the main uncertainty sources of the calibration method were analyzed.[2] Some researchers focused on the new application of the theodolite. Based on an immovable measuring coordinate system, a new 3D coordinate measurement system was described to avoid mutual collimation between the theodolites.[3] The bridge dynamic response monitoring system was accomplished using a high sampling-rate robotic total station.[4] Some researchers combined the established methods with theodolites while resolving the present disadvantages. Combining the traditional theodolite measurement principle of forward intersection and a camera, a novel precise guiding method for visual guiding theodolite measurements in volume space was reported.[5] In some studies, a camera is mounted on the theodolite or integrated in the theodolite as a single instrument. A universal and flexible theodolite-camera system in which a camera is mounted on the theodolite for making accurate measurements over large volumes was described.[6] Geo-monitoring using modern total stations and RGB + D images was proposed, and a camera is integrated in a total station.[7]

An autocollimator is also a non-contact, real time, and high precision instrument for small angle detection; thus, it is suitable for small angular displacement measurements, especially in precision metrology, industrial manufacturing, and aerospace fields.[8] Although the research on autocollimator has a long history, many studies are still focused on it.[9–16] A charge coupled device (CCD) is the detector for angle detection in autocollimators. Currently, the acquisition and pointing of the reflector are accomplished using theodolites manually. In the geo-monitoring applications, such as bridge dynamic response monitoring tasks, the theodolite fails to record the pointing angle of the reflector precisely when there is a reflector deviation caused by environmental interference. However, in this condition, the autocollimator is capable of measuring the small deviation of the reflector with high precision, typically a second of arc. Because both the autocollimator and theodolite depend on the laser optical beam to assist measurements, by combining the autocollimator and theodolite, an auto-collimation theodolite (ACT) can measure and monitor the pointing angle of the reflector precisely even when the reflector generates deviation.

a)E-mail: wangzhiqian@ciomp.ac.cn

Based on the principle of autocollimators and theodolites, this paper proposes the ACT for reflector automatic acquisition and pointing. The principle of auto-collimation and theodolites is reviewed first, and then the coaxial ACT structure is designed. Subsequently, the acquisition and pointing strategies based on the ACT are presented, which first quickly acquires the target over a wide range and then points the laser spot to the CCD zero position. A series of experiments are executed to verify the acquisition and pointing performance.

The structure of this paper is as follows. Section II presents the principle of the ACT. The acquisition and pointing strategies are described in Sec. III. Experimental results are conducted in Sec. IV. Section V concludes the paper.

II. PRINCIPLE

In this section, the principle of theodolites and autocollimators is introduced first, and then the structure of the ACT which combines a theodolite and an autocollimator is built.

A. The principle of theodolite

A theodolite is a precision instrument for angle determination in horizontal and vertical planes. The schematic view of using theodolites to measure the azimuth angle and elevation angle is shown in Fig. 1(a). Two perpendicular axes, namely, the vertical axis and the horizontal axis, are located in the rotation frame. The intersection point of the two axes is point O.

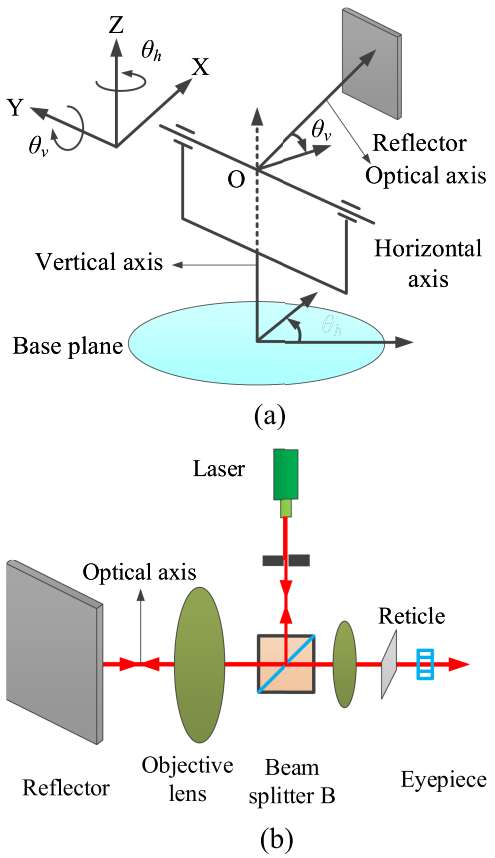

FIG. 1. Mechanical and optical structure of a theodolite. (a) Schematic view of a theodolite for azimuth angle θ_h and elevation angle θ_v measurements. (b) Optical structure of a theodolite.

In each axis, a rotary encoder is used to measure the rotation angle of the optical axis against the zero position. θ_h denotes the angle between the optical axis and the zero position of the horizontal encoder, and θ_h is also known as the azimuth angle. θ_v denotes the angle between the optical axis and the zero position of the vertical encoder, and θ_v is also known as the elevation angle. Theoretically, by rotating the optical axis along the horizontal axis (Y axis) and vertical axis (Z axis), the optical beam is capable of pointing to the entire space around point O. Traditional theodolites are rotated manually. With the development of control technology, motors are integrated into theodolites, and robotic theodolites emerged. Robotic theodolites are capable of rotating the optical axis along the horizontal and vertical axes automatically.

In pointing applications, the optical axis of theodolites is adjusted to ensure that the normal axis of the reflector is parallel to the optical axis. At this very moment, θ_h and θ_v are called pointing angles of the target. As shown in Fig. 1(b), the projected light beam is parallel to the reflected light beam, and the position of the reflected laser spot is at the center of the reticle. However, there are two shortcomings of the current theodolite. First, the pointing angles cannot be precisely calculated if the reflected beam is not located at the center of the reticle. Second, in order to obtain pointing angles, normally, people are involved in the target aiming process. Therefore, an autocollimator is integrated into the theodolite to solve the current disadvantages.

B. The principle of autocollimator

The schematic view of using autocollimators to measure two-axis angle is shown in Fig. 2. The system consists of a laser source, an objective lens, a reflector, and a CCD. The CCD is located at the focal position of the objective lens, and the focal length of the system is f. In practical applications, the mirror is mounted on the target as the reflector, and the target is called the cooperative target. The optical axis is parallel to the X axis. If the reflector has a deviation angle θ_y, then the reflected laser spot generates a horizontal displacement Δ_y on the CCD. Similarly, a deviation angle θ_z corresponds to a vertical displacement Δz. θ_y and θ_z are called deviation angles

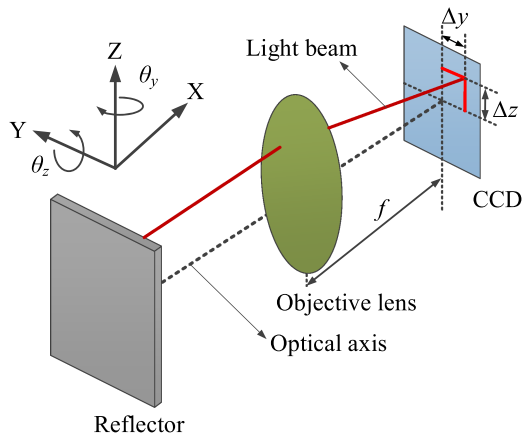

FIG. 2. Schematic view of auto-collimation measuring the angle θ_y and the angle θ_z of the reflector.

of the reflector. According to the principle of auto-collimation, the relationship between the deviation angles of the reflector and the displacements of the reflected beam on the CCD is described as

$$\begin{cases} \tan(2\theta_y) = \dfrac{\Delta y}{f} \\ \tan(2\theta_z) = \dfrac{\Delta z}{f}. \end{cases} \tag{1}$$

Using the Taylor expansion, Eq. (1) can be expressed as

$$\begin{cases} \theta_y = \dfrac{\Delta y}{2f} - \dfrac{1}{3}\left(\dfrac{\Delta y}{2f}\right)^3 + \dfrac{1}{5}\left(\dfrac{\Delta y}{2f}\right)^5 - \cdots \\ \theta_z = \dfrac{\Delta z}{2f} - \dfrac{1}{3}\left(\dfrac{\Delta z}{2f}\right)^3 + \dfrac{1}{5}\left(\dfrac{\Delta z}{2f}\right)^5 - \cdots. \end{cases} \tag{2}$$

Usually, the values of $\Delta y/(2f)$ and $\Delta z/(2f)$ are quite small, and then Eq. (2) approximately equals Eq. (3),

$$\begin{cases} \theta_y \approx \dfrac{\Delta y}{2f} \\ \theta_z \approx \dfrac{\Delta z}{2f}. \end{cases} \tag{3}$$

C. The principle of auto-collimation theodolite

Combining an autocollimator and a theodolite, an ACT is constructed. The autocollimator and the theodolite share the same optical axis. On the one hand, the ACT is capable of measuring the small angles (θ_y and θ_z) between the optical axis and the projected beam or reflected beam, i.e., the deviation angles of the reflector. On the other hand, the ACT is used to detect the angles (θ_h and θ_v) between the optical axis and the zero positions of the encoders; meanwhile, the ACT with integrated motors is used to rotate the optical axis to a specific position automatically. The optical pathway diagram of the ACT is shown in Fig. 3. The optical beam emitted from the laser is converted into a collimated optical beam through the beam splitter A, beam splitter B, and objective lens. If the reflector is in the field of view of the ACT, the collimated optical beam projected on the reflector is then reflected back to the objective lens. Some of the reflected optical beam directly goes through the beam splitter B and lens and then is focused on the reticle so that the laser spot can be seen from the eyepiece. The rest of the reflected optical beam is reflected by the beam splitter B, passes the beam splitter A and lens, and then produces a laser spot on the CCD.

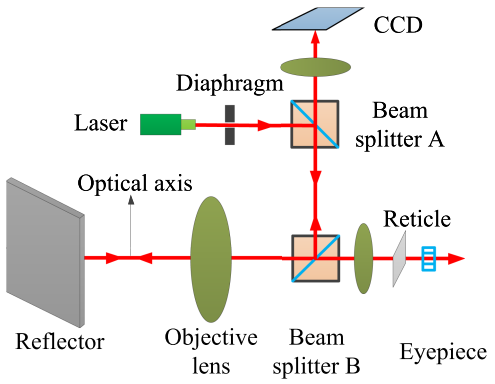

FIG. 3. Optical pathway diagram of the collimation theodolite.

When the reflected optical beam is in the center of the reticle, the angle between the zero position of the encoder and the optical axis is defined as the pointing angle; in this scenario, the laser spot on the CCD is defined as the CCD zero position. θ_{ph} and θ_{pv} are used to denote the pointing angles of the reflector in the horizontal direction and vertical direction, respectively. In our system, as can be seen in Fig. 1, $\theta_h \geq 0$ ($\theta_h < 0$) when the reflector is rotated along the Z axis counterclockwise (clockwise) and $\theta_v \geq 0$ ($\theta_v < 0$) when the reflector is rotated along the Y axis clockwise (counterclockwise). In Fig. 2, $\theta_y \geq 0$ ($\theta_y < 0$) when the reflector is rotated along the Z axis clockwise (counterclockwise) and $\theta_z \geq 0$ ($\theta_z < 0$) when the reflector is rotated along the Y axis counterclockwise (clockwise). Usually, the values of θ_y and θ_z are much smaller than those of θ_h and θ_v; thus, θ_{ph} and θ_{pv} are expressed as

$$\begin{cases} \theta_{ph} = \theta_h - \theta_y \\ \theta_{pv} = \theta_v - \theta_z. \end{cases} \tag{4}$$

As can be seen from Eq. (4), the pointing angles are calculated by the combination of the encoder values (θ_h and θ_v) and auto-collimation angles (θ_y and θ_z). In Sec. III, we focus on the measurement of pointing angles using the ACT.

III. THE STRATEGIES FOR ACQUISITION AND POINTING

The combination of the theodolite and autocollimator guarantees high precision of pointing for two reasons. First, the measurement accuracy of the encoder (theodolite) is reached within seconds of arc. Second, the principle of auto-collimation ensures its high measurement accuracy, typically a second of arc. However, the field of view of the ACT is usually in the level of $1000'' \times 1000''$,[17,18] thus raising difficulties for the reflector acquisition and pointing.

The strategies for acquisition and pointing are shown in Fig. 4. Several sensors are included to achieve the acquisition and pointing processes. The pixel number and position of the reflected laser spot are recorded by the CCD. Here, P_n denotes the pixel number, and P_p represents the position. According to the values of P_n and P_p and the scan flag bit S_f, the acquisition and pointing processes are determined. P_a is the threshold value for acquisition, that is to say, the acquisition process is accomplished when $P_n \geq P_a$ is detected. y_0 and z_0 are the zero positions of the laser spot in the horizontal and vertical directions on the CCD, respectively. In order to determine the status of the scan flag, P_n and P_a should be calculated first. Since the laser spot on the CCD contains both the intensity of the background noise and the spot itself, the threshold centroid method is used to calculate the pixel number and coordinate of the laser spot. The threshold calculation method can be expressed as[19]

$$I(i,j) = \begin{cases} I(i,j), I(i,j) > I_{th} \\ 0, I(i,j) \leq I_{th}, \end{cases} \tag{5}$$

where i and j are the pixel coordinates in the horizontal and vertical directions; $I(i, j)$ is the intensity of the pixel on the

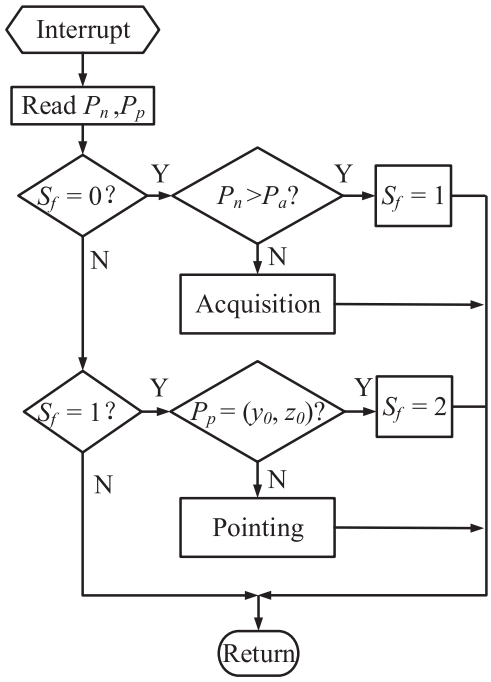

FIG. 4. Program flow chart of acquisition and pointing of the ACT.

CCD; I_{th} is the threshold value. Using Eq. (5), the intensity of the image lower than the threshold value I_{th} is filtered; thus, the background noise from the fluorescent lamp or other sources can be immensely decreased and the position stability of the laser spot can be dramatically increased. P_n is equal to the sum of all the pixels whose intensity is bigger than I_{th}. Then the gray centroid of the laser spot expressed in discrete form is

$$\begin{cases} y = \dfrac{\sum\limits_{(i,j)\in s} iI(i,j)}{\sum\limits_{(i,j)\in s} I(i,j)} \\ z = \dfrac{\sum\limits_{(i,j)\in s} jI(i,j)}{\sum\limits_{(i,j)\in s} I(i,j)}, \end{cases} \tag{6}$$

where S is the area of the image; y and z are the horizontal and vertical coordinates of the laser spot. Based on the values of P_n and P_p, the scan flag bit S_f is set. When $S_f = 0$, if $P_n \geq P_a$, S_f is set as 1; otherwise, acquisition subprogram is executed. When $S_f = 1$, if $P_p = (y_0, x_0)$, S_f is set as 2; otherwise, pointing subprogram is executed. The acquisition and pointing modes will be discussed in Secs. III A and III B.

A. Acquisition mode of ACT

Since the field of view of the ACT is quite small, the ACT should be placed at a suitable position. In other words, the angle of the optical axis against the normal axis of the reflector should be small. In acquisition mode, the ACT searches the reflector in a relative large volume. As shown in Fig. 5, in order to capture the reflector quickly, the acquisition mode includes coarse acquisition and fine acquisition. The scan speeds of coarse acquisition and fine acquisition are v_c ($''$ s^{-1}) and v_f ($''$ s^{-1}), respectively. The speed of coarse acquisition is much

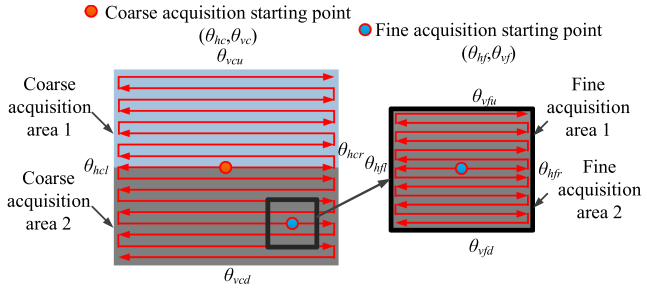

FIG. 5. Scan path of coarse acquisition and fine acquisition.

faster than that of fine acquisition. The starting point of coarse acquisition is $(\theta_{hc}, \theta_{vc})$, and the scan area is divided into area 1 and area 2. The top, bottom, left, and right boundaries in area 1 are θ_{vcu}, θ_{vc}, θ_{hcl}, and θ_{hcr}, respectively. The top, bottom, left, and right boundaries in area 2 are θ_{vcd}, θ_{hcl}, and θ_{hcr}, respectively. Area 1 is scanned first, and then area 2 is followed. The search area division approach is easy to implement and ensures full range search around the center. In this mode, $S_f = 0$ and the pixel number of the laser spot on the CCD is recorded every T ms. In other words, the scan area is v_cT/1000 ($''$) in every T ms. If $P_n \geq P_c$ (pixel number threshold for coarse acquisition) is detected, coarse acquisition is successful, and then fine acquisition follows. When coarse acquisition is completed, it means a small part of the reflected optical beam is projected on the CCD. In other words, the angle between the optical axis and the normal axis of the reflector is small. Therefore, a small range of scanning is capable of receiving the large part of the reflected optical beam. The starting point of fine acquisition $(\theta_{hf}, \theta_{vf})$ is the stop point of coarse acquisition. The boundary of fine acquisition is much smaller than that of coarse acquisition. Similarly, the scan area is split into two parts. In fine acquisition area 1, the top, bottom, left, and right boundaries are θ_{vfu}, θ_{vf}, θ_{hfl}, and θ_{hfr}, respectively. In fine acquisition area 2, the top, bottom, left, and right boundaries are θ_{vf}, θ_{vfd}, θ_{hfl}, and θ_{hfr}, respectively. The scan area is v_fT/1000 ($''$) in every T ms at fine acquisition mode, and the acquisition is completed when $P_n \geq P_a$ is detected. At this stage, using Eq. (4), pointing angles are obtained. In some applications, only the pointing angles are needed. However, it requires the optical axis to be parallel to the normal axis of the reflector sometimes.

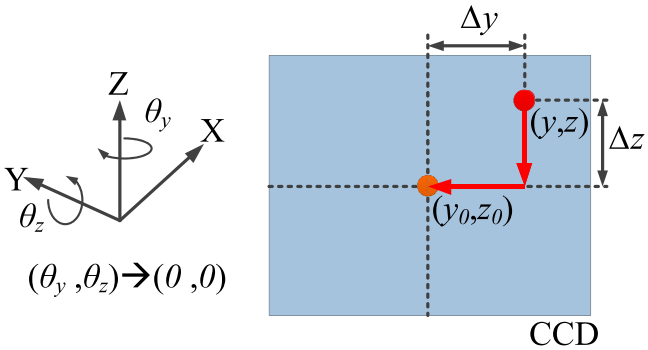

FIG. 6. Laser spot trajectories of the pointing mode on the CCD, i.e., the laser spot is moved from (y, z) to (y_0, z_0).

B. Pointing mode of ACT

In ideal conditions, the pointing mode is used to decrease the collimation angles from (θ_y, θ_z) to (0, 0), i.e., the laser spot on the CCD is moved from (y, z) to zero position (y_0, z_0), as shown in Fig. 6. Usually, the accuracy of the high precision autocollimator is less than 1″ so that the scan speed of the ACT should take the measurement accuracy of the CCD into account. In pointing mode, the scan velocity is v_p, and the moved angle is v_pT/1000 (″) every T ms. In practical conditions, small angles θ_{yth} and θ_{zth} are set and the pointing mode is completed when $\theta_y \le \theta_{yth}$ and $\theta_z \le \theta_{zth}$ are achieved.

IV. EXPERIMENTS

A series of experiments are conducted to test the described method using the prototype of the ACT. In order to improve the measurement accuracy of the ACT, a calibration experiment is executed first. Then the acquisition and pointing experiments of the ACT are carried out. In our experiment, a total station TS15 is used as the theodolite. Its angle measurement accuracy in horizontal and vertical directions is reached at 1″, and the display resolution is 0.1″. Two motors are integrated in the theodolite. The dimension of CCD is 752 H × 480 V, and the pixel size of CCD is 6 μm × 6 μm.

A. Calibration

As shown in Eq. (4), the pointing angles are the combination of theodolite measurement (θ_h, θ_v) and collimation measurement (θ_y, θ_z). θ_h and θ_v can be directly obtained from the rotary encoders. θ_y and θ_z are calculated using the relationship between the focal length of the optical system and the displacements of the laser spot on the CCD, i.e., the relationship in Eq. (1). In order to calculate θ_y and θ_z accurately, normally, the focal length f should be calibrated first. Based on Eq. (2), the relationship between reflector deviations and the displacements of the laser spot on the CCD is calibrated using linear polynomials,

$$\begin{cases} \theta_y = k_1 \Delta y + k_0 \\ \theta_z = k_3 \Delta z + k_2, \end{cases} \tag{7}$$

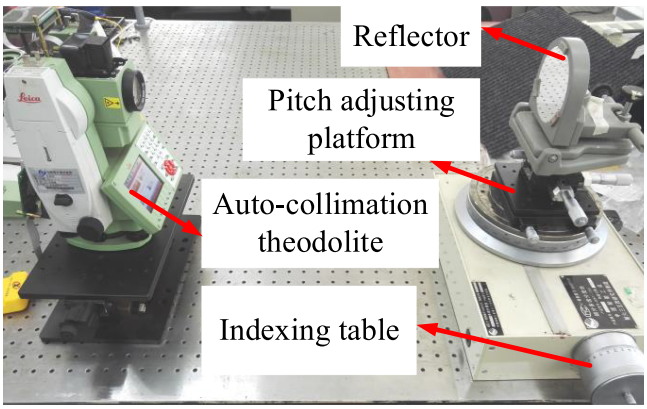

FIG. 7. Calibration setup of k_3, k_2, k_1, and k_0.

where θ_y and θ_z denote the deviation angles of the reflector; k_3, k_2, k_1, and k_0 are calibration coefficients; Δy and Δz are the displacements of the laser spot. The position of the CCD is located at the focal point of the reflected optical path, as shown in Fig. 3. The calibration setup is shown in Fig. 7, and it consists of a reflector, a pitch adjusting platform, an indexing table, and an ACT. The calibration procedure of k_3, k_2, k_1, and k_0 includes the following steps:

- Aim the reflector through the ACT using the eyepiece and make sure that the optical beam is projected on the center of the reflector. Meanwhile, the reflected beam is located at the center of the reticle. Record the coordinate of the laser spot (y_0, z_0) on the CCD and set the current deviation angles of the reflector as (0″, 0″).
- Rotate the reflector along the Z axis using the indexing table (accuracy 1″) from 0″ to 100″ and 0″ to −100″ with the interval of 10″; each deviation value θ_y corresponds to a laser spot displacement Δy on the CCD.
- Rotate the reflector along the Y axis using the pitch adjusting platform (accuracy 1″) from 0″ to 100″ and 0″ to −100″ with the interval of 10″; each deviation value θ_z corresponds to a laser spot displacement Δz on the CCD.

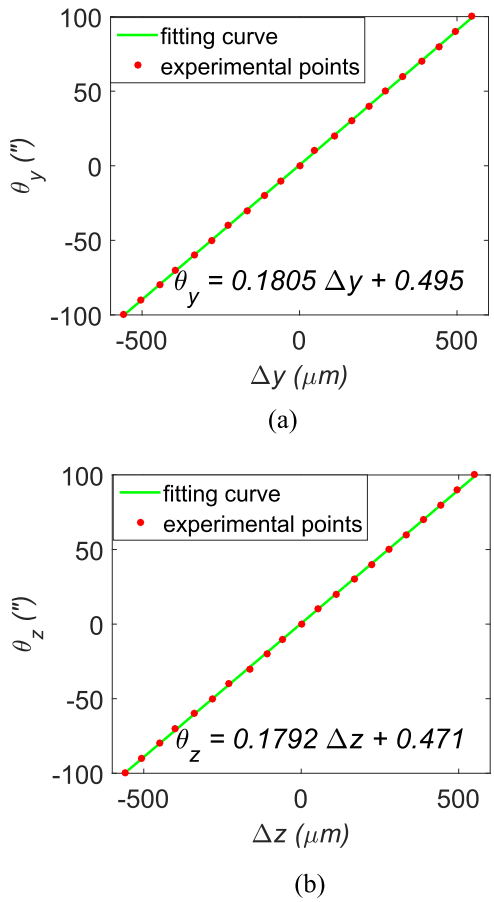

FIG. 8. Linear polynomial fitting between deviation angles of the reflector and the laser spot displacements on the CCD. (a) Calibration results of k_1 and k_0. (b) Calibration results of k_3 and k_2.

TABLE I. Acquisition mode in the horizontal direction and vertical direction.

Run	θ_h	θ_y	θ_{ph}	θ_v	θ_z	θ_{pv}
1	104°27′31.6″	55.3″	104°26′36.3″	91°9′52.4″	−26.9″	91°10′19.3″
2	104°25′25.3″	−72″	104°26′37.3″	91°10′37.6″	16.3″	91°10′21.3″
3	104°26′43.2″	6.7″	104°26′36.5″	91°9′55.7″	−26.5″	91°10′22.2″
4	104°25′48.0″	−38.8″	104°26′36.8″	91°11′9.5″	49.2″	91°10′20.3″
5	104°26′27.8″	−9.1″	104°26′36.9″	91°10′27.3″	7.7″	91°10′19.6″
6	104°25′23.5″	−71.2″	104°26′34.7″	91°11′36.6″	74.7″	91°10′20.9″
7	104°26′31.7″	−5.2″	104°26′36.9″	91°9′45.2″	−35.5″	91°10′20.7″
8	104°27′11.2″	32.7″	104°26′38.5″	91°9′43.1″	−38.9″	91°10′22.0″
9	104°26′48.3″	10.8″	104°26′37.5″	91°10′28.4″	8.8″	91°10′19.6″
10	104°27′34.0″	58.6″	104°26′35.4″	91°11′10.1″	49.6″	91°10′20.5″

TABLE II. Pointing mode in the horizontal direction and vertical direction.

Run	θ_h	θ_y	θ_{ph}	θ_v	θ_z	θ_{pv}
1	104°26′36.5″	0.3″	104°26′36.2″	91°10′19.1″	−0.8″	91°10′19.9″
2	104°26′36.8″	−0.2″	104°26′37.0″	91°10′21.6″	0.5″	91°10′21.1″
3	104°26′36.8″	0.5″	104°26′36.3″	91°10′21.9″	−0.1″	91°10′22″
4	104°26′36.4″	−0.2″	104°26′36.6″	91°10′20.7″	0.3″	91°10′20.4″
5	104°26′35.7″	−0.9″	104°26′36.6″	91°10′20.5″	0.7″	91°10′19.8″
6	104°26′34.6″	−0.5″	104°26′35.1″	91°10′20.7″	0.2″	91°10′20.5″
7	104°26′36.3″	−0.7″	104°26′37.0″	91°10′19.4″	−0.9″	91°10′20.3″
8	104°26′39.1″	0.9″	104°26′38.2″	91°10′21.3″	−0.6″	91°10′21.9″
9	104°26′38.2″	0.4″	104°26′37.8″	91°10′20.2″	0.5″	91°10′19.7″
10	104°26′36.5″	0.7″	104°26′35.8″	91°10′20.8″	0.2″	91°10′20.6″

Using Eq. (7) to fit k_3, k_2, k_1, and k_0, the fitting results are shown in Fig. 8. It can be seen that $k_1 = 0.1805$ and $k_0 = 0.495$, thus $\theta_y = 0.1805\Delta y + 0.495$. $k_3 = 0.1792$ and $k_2 = 0.471$, thus $\theta_z = 0.1792\Delta z + 0.471$.

Comparing Eqs. (3) and (7) and keeping in mind that the units need to be unified, the focal length f can be calculated and f = 573 mm. Substituting focal length f by 573 mm and pixel size by 6 μm into Eq. (3), the resolution of the CCD is 1.08″. Similarly, the field of view of the CCD is 2*406″ H × 2*259″ V. The threshold centroid method in Eqs. (5) and (6) can further improve the resolution of pixel localization to 0.5 pixel, i.e., the CCD resolution reaches 0.5″. The control accuracy of our system is 1″. Based on error propagation theory, the pointing resolution is about 1″.

B. Comparison of acquisition mode and pointing mode

As described in Sec. III, in acquisition mode, the laser spot can be located anywhere on the CCD, i.e., the collimation angles θ_y and θ_z have relatively large values; in pointing mode, the laser spot is located at the zero position of the CCD, thus θ_y and θ_z are quite small. In this section, the pointing angles of acquisition mode and pointing mode are explored. The coarse acquisition scan speed v_c is set as 12 000″ s^{-1}; thus, the image on the CCD is recorded every 5 ms when the optical axis moves 60″. The coarse acquisition pixel threshold value P_c is set as 50. The fine acquisition scan speed v_f is 4000″ s^{-1}; thus, the image on the CCD is recorded every 5 ms when the optical axis moves 20″, and the fine acquisition pixel threshold value P_a is set as 1000. v_p is 200″ s^{-1}, and both θ_{yth} and θ_{zth} are set as 1″. In this series of experiments, the position of the reflector is fixed, and the horizontal and vertical angles of the ACT are slightly changed (both horizontal and vertical directions are less than 3°); the acquisition and pointing results in 10 runs are shown in Tables I and II.

As can be seen in Table I, in acquisition mode, the average of pointing angles in the horizontal direction θ_{ph} is 104°26′36.7″, and the corresponding standard deviation is

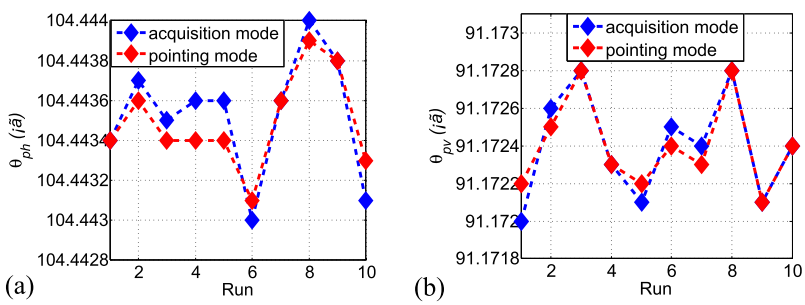

FIG. 9. Pointing angles calculated using encoder values and auto-collimation angles in acquisition mode and pointing mode. (a) Pointing angles in the horizontal direction. (b) Pointing angles in the vertical direction.

3.3″ (3σ). The average of pointing angles in the vertical direction θ_{pv} is 91°10′20.6″, and the corresponding standard deviation is 3″ (3σ).

As can be seen in Table II, in pointing mode, the average of pointing angles in the horizontal direction θ_{ph} is 104°26′36.6″, and the corresponding standard deviation is 2.7″ (3σ). The average of pointing angles in the vertical direction θ_{pv} is 91°10′20.6″, and the corresponding standard deviation is 2.4″ (3σ). Compared with the acquisition mode, the pointing mode has several advantages. First, the nonlinear error of CCD measurements is largely eliminated when the laser spot is at the zero position. Therefore, the measurement accuracy is higher than that of the acquisition mode. Second, even if the deviation angle of the reflector is slightly changed, the pointing mode is capable of detecting the target pointing angle (Fig. 9).

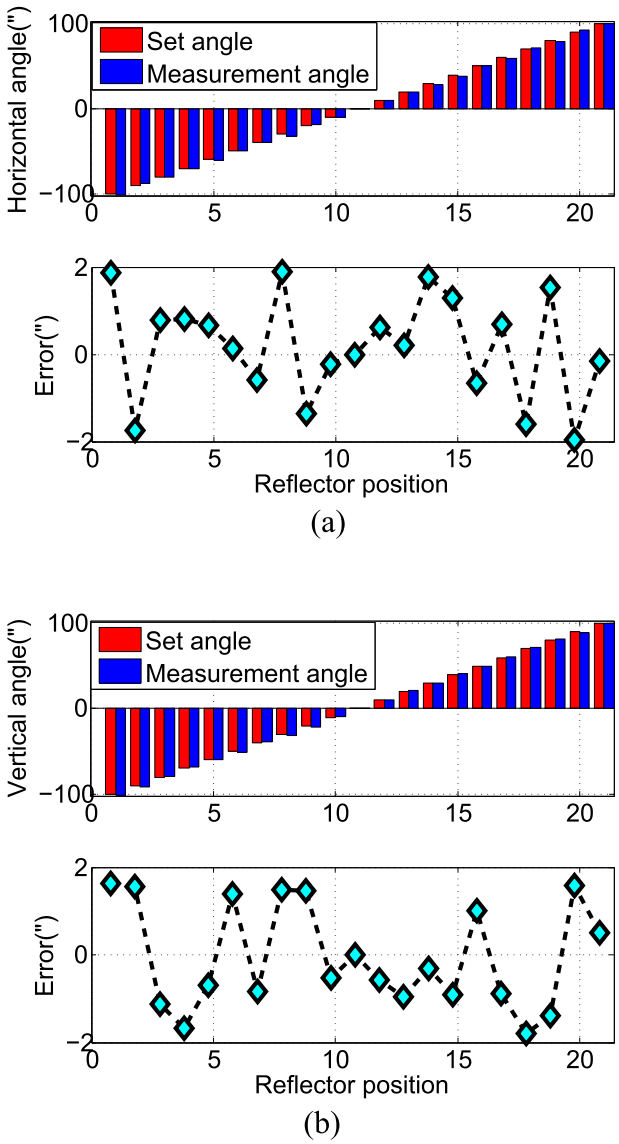

FIG. 10. Pointing mode experiments when the reflector is rotated from −100″ to 100″ both in horizontal and vertical directions. (a) Measurement results in the horizontal direction. (b) Measurement results in the vertical direction.

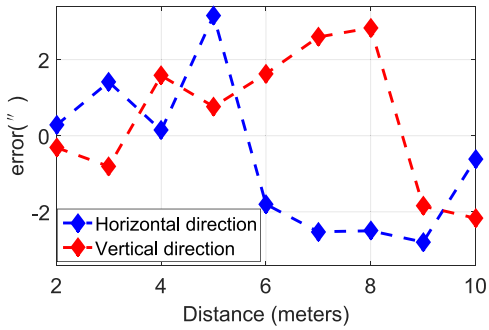

FIG. 11. Measurement distance between the reflector and the ACT is increased from 2 m to 10 m with the interval of 1 m.

C. Measurement accuracy in horizontal and vertical directions

In this part, the accuracy of the proposed system is tested. First, at a distance of 2 m, the measurement accuracy in the horizontal direction is tested. The reflector is rotated along the Z axis from 0″ to 100″ and 0″ to −100″ with an interval of 10″, and 20 positions are measured in total. The set value is obtained by aiming the reflector using the eyepiece of the ACT. In each position, the ACT automatically points to the reflector, and the angles θ_h and θ_y are recorded. Similarly, the measurement accuracy in the vertical direction is tested. θ_v and θ_z are recorded at each position. The measurement results are shown in Fig. 10. From Figs. 10(a) and 10(b), it can be seen that the measurement angle follows the set angle well in the range of −100″ to 100″. In horizontal and vertical directions, the system measurement errors are less than ±2″.

Second, the measurement distance between the reflector and the ACT is increased from 2 m to 10 m with the interval of 1 m. Similarly, the set values are obtained by aiming the reflector using the eyepiece of the ACT, and the measurement values are achieved by the ACT automatically. Figure 11 shows the measurement error in horizontal and vertical directions. As can be seen in Fig. 11, the maximum errors in horizontal and vertical directions are less than 3.2″ and 2.9″, respectively. In the horizontal direction, the maximum value of the error is at 5 m rather than 10 m, and the maximum value of the error is at 8 m in the vertical direction. The reason is that the auto-collimation measurement is not sensitive to the measurement distance. However, if the temperature or airflow fluctuates, the measurement error grows as the distance increases.

V. CONCLUSION

This paper presents an approach of pointing reflectors combining the principle of theodolites and auto-collimation. The prototype of the ACT is capable of automatic measuring the angles between the reflector's normal axis and the zero position of rotary encoders. The pointing angle measurement accuracy with arc seconds is achieved by subtracting the auto-collimation angle from the rotary encoder value. Because both autocollimators and theodolites depend on the laser optical beam to assist measurements, the former can be easily integrated in the latter by sharing the optical path. The ACT

enhances the autocollimator's performance by achieving deviation angle automatic measuring, and the ACT strengthens the theodolite's performance by achieving automatic monitoring. The applications of the ACT include (1) deformation measurements such as structure health monitoring,[20] precision manufacturing,[21] and precision alignment; (2) directional aiming measurements used in coal mining and tunnel excavation combined with a north finder.[22]

ACKNOWLEDGMENTS

This work is supported by the Major Scientific and Technological Project of Jilin Province, China (Nos. 20150204013GX and 20160204053GX).

[1]L. Šiaudinytė and H. S. Suh, Measurement **67**, 177 (2015).
[2]L. Šiaudinytė and K. T. V. Grattan, Measurement **86**, 276 (2016).
[3]Z. Sun, Z. Wang, H. Zhai, and X. Yang, Meas. Sci. Technol. **24**, 055001 (2013).
[4]J. Yu, P. Zhu, B. Xu, and X. Meng, Measurement **104**, 60 (2017).
[5]B. Wu and X. Su, Opt. Int. J. Light Electron Opt. **126**, 3969 (2015).
[6]X. Zhang, Z. Zhu, Y. Yuan, L. Li, X. Sun, Q. Yu, and J. Ou, Opt. Lasers Eng. **50**, 1611 (2012).
[7]A. Wagner, Measurement **82**, 64C74 (2016).
[8]Y. Saito, Y. Arai, and W. Gao, Sens. Actuators, A **150**, 175 (2009).
[9]K. Fujimaki and K. Mitsui, Opt. Eng. **47**, 013602 (2008).
[10]R. Liu, X. Guo, J. Yu, Y. Qin, Q. Bian, and W. Li, Opt. Int. J. Light Electron Opt. **124**, 1132 (2013).
[11]K. Ishikawa, T. Takamura, M. Xiao, S. Takahashi, and K. Takamasu, Meas. Sci. Technol. **25**, 064008 (2014).
[12]T. Yandayan, S. A. Akgoz, and M. Asar, Meas. Sci. Technol. **25**, 015010 (2014).
[13]B. Liu, B. Li, A. Tian, H. Yang, F. Gao, and L. Chen, Meas. Sci. Technol. **26**, 015203 (2015).
[14]B. Wu, F. Yang, W. Ding, and T. Xue, Rev. Sci. Instrum. **87**, 035102 (2016).
[15]T. Yandayan, R. D. Geckeler, M. Aksulu, S. A. Akgoz, and B. Ozgur, Rev. Sci. Instrum. **87**, 051903 (2016).
[16]Y. Shimizu, S. L. Tan, D. Murata, T. Maruyama, S. Ito, Y. L. Chen, and W. Gao, Opt. Express **24**, 2788 (2016).
[17]L. Wang, L. Liu, J. Sun, Y. Zhou, Z. Luan, and D. Liu, Opt. Int. J. Light Electron Opt. **121**, 1614 (2010).
[18]I. A. Konyakhin and T. V. Turgalieva, J. Opt. Technol. **80**, 772 (2013).
[19]K. Li, C. Kuang, and X. Liu, Rev. Sci. Instrum. **84**, 015108 (2013).
[20]A. Sabato, C. Niezrecki, and G. Fortino, IEEE Sens. J. **17**, 226 (2017).
[21]W. Gao, S. W. Kim, H. Bosse, H. Haitjema, Y. L. Chen, X. D. Lu, W. Knapp, A. Weckenmann, W. T. Estler, and H. Kunzmann, CIRP Ann. **64**, 773 (2015).
[22]J. Luo, Z. Wang, C. Shen, A. Kuijper, Z. Wen, and S. Liu, Sensors **16**, 1513 (2016).